Guidance Law Design for Tracking Mobile Ground Targets Using An Unmanned Aerial Vehicl with A Fixed Camera

Liang Sun[1] and Daniel Pack[2]

***Abstract*— In this paper, we present two novel guidance laws for an unmanned aerial vehicle (UAV) equipped with a fixed camera to track a mobile ground target. The system dynamics is established in the level local coordinate frame, removing the need of converting the target location information to the global inertial frame. The first guidance law is developed using backstepping technique requiring the estimation of target-to-UAV range information, which is provided by an extended Kalman filter (EKF). The observability analysis reveal the flaw of the range-based approach. An alternative guidance law is then developed using the sliding-mode technique, which does not require the target-to-UAV range information. Simulations results show the effectiveness and comparison of the two guidance laws. Estimation results aligns with the observability analysis.**

I. Introduction

We have witnessed an increasing interest in the development of Unmanned Aerial Vehicles (UAVs), in the context of a variety of applications, such as Intelligence, Reconnaissance and Surveillance (ISR), search and rescue, border control, law enforcement, and disaster/battlefield damage assessment, among many others. Most of these applications are defined with respect to the ground environment. Tracking mobile ground targets, therefore, becomes an essential capability for UAVs to accomplish those missions. For such tasks, fixed-wing UAVs outperform helicopters to reach high speeds at low energy consumption, while their dynamics constrains the visibility of the ground target. The advance of optical sensors (video cameras) enables a passive, lightweight, inexpensive sensing component to be equipped on UAVs to capture the information on the ground. To accommodate the mobility of ground targets, gimbals are usually used to decouple camera rotation from the motion of UAVs. However, the extra payload, cost and control efforts induced by the gimbal confine the UAV flight duration, especially for miniature and micro UAVs. In this paper, we seek to conduct mobile target tracking using a small fixed-wing UAV equipped with a fixed (non-gimbaled) camera. The coupled UAV-camera dynamics calls for sophisticated navigation, guidance and control algorithms and robust motion estimation techniques to compensate unknown target movement.

To address the problem, we divide the overall tracking process into two segments, as shown in Figure 1: an initial segment, generated by a path planner, that optimizes the vehicle trajectory to reach a desired target-relative location from some initial point for the UAV to initially capture the target in its sensor field-of-view (FOV), and the second segment when the UAV maintains, for the most part, the ground target in its sensor FOV. In our previous work [1], we proposed a dynamic-horizon-based optimal path planning approach to regulate the UAV in the initial segment. In this paper, we focus on the guidance of the UAV in the second segment. This task can be considered as a vision-based target tracking problem, in which the camera motion is tightly coupled with the UAV motion. The guidance law that focuses on the second segment of UAV path uses a stream of camera images captured by a video sensor mounted on the nose of the UAV.

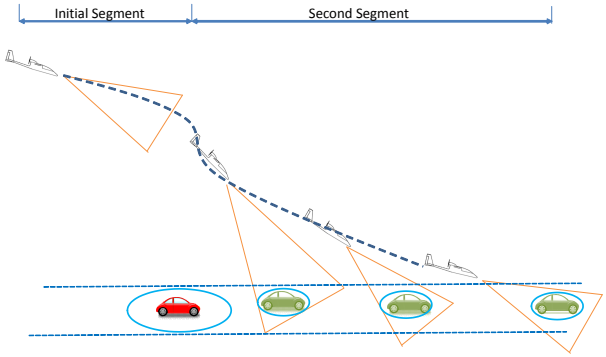

Fig. 1: An Unmanned Aerial Vehicle (UAV) with a fixed video camera tracks a mobile ground target while experiences initial and second segments of the process.

In the literature, most of the work for tracking mobile ground targets using a UAV was conducted based on gimbaled sensors [2], [3], [4], [5], [6]. Several studies for target tracking using non-gimbaled cameras have also been reported. In [7], two fixed cameras were equipped on a single UAV, in which the forward-looking camera is used to perceive obstacles in the UAV flight path and downward-looking camera is used to follow a roadway. In [8], a path-planning algorithm was proposed to maximize the observation time on a target, whose position is assumed to be known at all time. In [9], a fixed camera pointing out the wing of a miniature aerial vehicle was used to track a stationary ground target. A nonlinear image-based feedback guidance strategy was developed to maintain the target in the FOV of the camera. However, to the best of our knowledge, no work has been reported on the development of the guidance law for tracking mobile targets using a small fixed-wing UAV equipped with

[1]Liang Sun is with Department of Mechanical and Aerospace Engineering, New Mexico State University, Las Cruces, NM, USA, 88003. lsun@nmsu.edu

[2]Daniel Pack is with College of Engineering and Computer Science, University of Tennessee at Chattanooga, Chattanooga, TN 37403. Daniel-Pack@utc.edu

a forward-facing non-gimbaled camera.

In this paper, we first introduce the coordinate frames used for the derivation of the system dynamics. It is followed by a three dimensional UAV-target kinematic model description with respect to an inertial coordinate frame onboard the UAV. The model is used to develop a novel Lyapunov-based nonlinear guidance law to direct the UAV motion to push a ground target toward the center of its captured images with the help of an Extended Kalman Filter (EKF) estimating the UAV-to-target range. An observability analysis showed a poor performance of the EKF's ability to estimate the UAV-to-target range when the target remains at the center of FOV, and an alternative innovative guidance law, based on a slide mode control technique, was developed accordingly.

The reminder of the paper is structured as follows. Section II introduces the coordinate frames used in the system dynamics. The UAV dynamics and target-UAV relative kinematics are presented in Section III. In Section IV, we present the development of the guidance law using UAV-to-target range information, provided by an EKF, and associated observability analysis for the EKF performance. The derivation of another guidance law without using the range information is presented in Section V. Simulation results are presented in Section VI, and Section VII concludes the work.

II. Coordinate frames

Guidance laws for UAVs to track mobile targets can be classified in two categories: global and local guidance laws. Global guidance laws require complete knowledge about the overall environment and target coordinates are typically represented in a global inertial frame. Path planning algorithms are typically developed by aligning the line of sight of the camera with the target-UAV vector, as shown in Figure 2. Local guidance laws, one that we present in this report, adopt a local inertial frame such as a camera coordinate frame, to estimate relative vehicle movements. The benefits of using local guidance laws are computational efficiency, involving fewer coordinate frames and inherent ability to operate without global knowledge of an operational environment. We next introduce, briefly, coordinate frames associated with system dynamics: an inertial frame, a vehicle frame, a vehicle-1 frame, a vehicle-2 frame, a body frame, a gimbal frame, and a camera frame.

A. The inertial frame $\mathcal{F}^i$

The inertial coordinate system is an earth-fixed coordinate system with its origin at a pre-defined location. In this report, this coordinate system is referred to as the North-East-Down (NED) reference frame. It is common for North to be referred to as the inertial x direction, East to be referred to as the inertial y direction, and down to be referred to as the inertial z direction.

B. The vehicle frame $\mathcal{F}^v$

The origin of the vehicle frame is at the center of mass of the UAV. However, the axes of $\mathcal{F}^v$ are aligned with the axes of the inertial frame $\mathcal{F}^i$. In other words, the unit vector $\mathbf{i}^v$ points North, $\mathbf{j}^v$ points East, and $\mathbf{k}^v$ points toward the center of the earth.

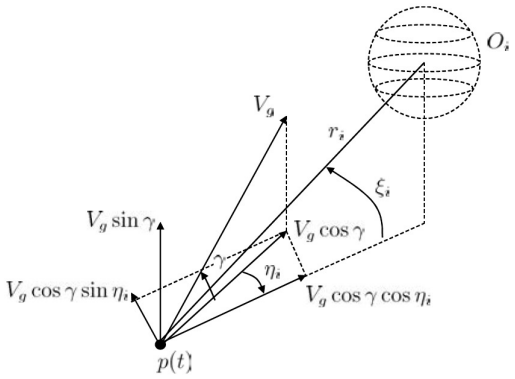

Fig. 2: A spherical frame.

C. The vehicle-1 frame $\mathcal{F}^{v1}$

The origin of the vehicle-1 frame is identical to the vehicle frame. However, $\mathcal{F}^{v1}$ is rotated in the positive right-handed direction about $\mathbf{k}^v$ by the heading (or yaw) angle, ψ. The transformation from $\mathcal{F}^v$ to $\mathcal{F}^{v1}$ is given by

$$\mathbf{p}^{v1} = R_v^{v1}(\psi)\,\mathbf{p}^v,$$

where

$$R_v^{v1}(\psi) = \begin{pmatrix} \cos\psi & \sin\psi & 0 \\ -\sin\psi & \cos\psi & 0 \\ 0 & 0 & 1 \end{pmatrix}.$$

D. The vehicle-2 frame $\mathcal{F}^{v2}$

The origin of the vehicle-2 frame is again the center of mass of the UAV and is obtained by rotating the vehicle-1 frame in a right-handed rotation about the $\mathbf{j}^{v1}$axis by the pitch angle, θ. The transformation from $\mathcal{F}^{v1}$ to $\mathcal{F}^{v2}$ is given by

$$\mathbf{p}^{v2} = R_{v1}^{v2}(\psi)\,\mathbf{p}^{v1},$$

where

$$R_{v1}^{v2}(\theta) = \begin{pmatrix} \cos\theta & 0 & -\sin\theta \\ 0 & 1 & 0 \\ \sin\theta & 0 & \cos\theta \end{pmatrix}.$$

E. The body frame (vehicle-3 frame) $\mathcal{F}^b$

The body frame is obtained by rotating the vehicle-2 frame in a right-handed rotation about iv2 by the roll angle, ϕ. The transformation from $\mathcal{F}^{v2}$ to $\mathcal{F}^b$ is given by

$$\mathbf{p}^b = R_{v2}^b(\phi)\,\mathbf{p}^{v2},$$

where

$$R_{v2}^b(\theta) = \begin{pmatrix} 1 & 0 & 0 \\ 0 & \cos\phi & \sin\phi \\ 0 & -\sin\phi & \cos\phi \end{pmatrix}.$$

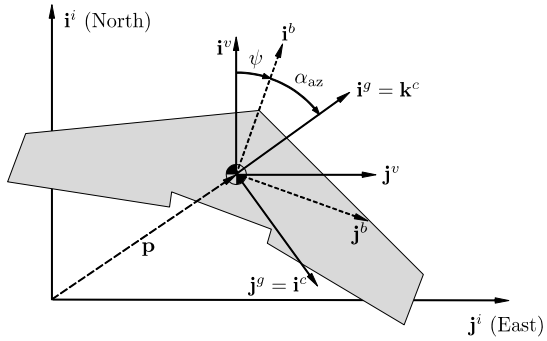

(a) Top-down view of coordinate frames.

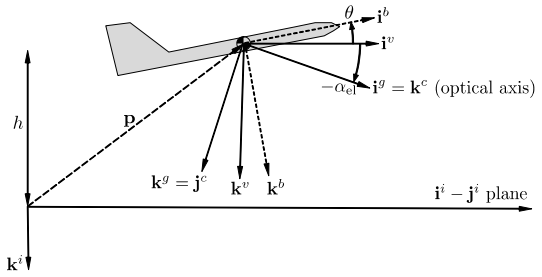

(b) Side view of coordinate frames.

Fig. 3: Coordinate frames: Inertial frame: $\mathcal{F}^i = \left(\mathbf{i}^i, \mathbf{j}^i, \mathbf{k}^i\right)$, Vehicle frame: $\mathcal{F}^v = (\mathbf{i}^v, \mathbf{j}^v, \mathbf{k}^v)$, Body frame: $\mathcal{F}^b = \left(\mathbf{i}^b, \mathbf{j}^b, \mathbf{k}^b\right)$, Gimbal frame: $\mathcal{F}^g = (\mathbf{i}^g, \mathbf{j}^g, \mathbf{k}^g)$, and Camera frame: $\mathcal{F}^c = (\mathbf{i}^c, \mathbf{j}^c, \mathbf{k}^c)$ [10].

F. The gimbal frame $\mathcal{F}^g$ and the camera frame $\mathcal{F}^c$

The coordinate frames shown in Figure 3 are used to derive rotation matrices R_b^g and R_g^c, which transform a vector from the body frame to the gimbal frame and from the gimbal frame to the camera frame, respectively, which are given by

$$R_b^g \triangleq \begin{pmatrix} \cos\alpha_{el}\cos\alpha_{az} & \cos\alpha_{el}\sin\alpha_{az} & -\sin\alpha_{el} \\ -\sin\alpha_{az} & \cos\alpha_{az} & 0 \\ \sin\alpha_{el}\cos\alpha_{az} & \sin\alpha_{el}\sin az & \cos\alpha_{el} \end{pmatrix}, \tag{1}$$

$$R_g^c \triangleq \begin{pmatrix} 0 & 1 & 0 \\ 0 & 0 & 1 \\ 1 & 0 & 0 \end{pmatrix}, \tag{2}$$

where α_{el} and α_{az} are elevation and azimuth angles of the gimbal. For the application of a non-gimbaled camera, both R_b^g and R_g^c are constant matrices, reflecting fixed coordinate relationships.

III. Dynamic Model

To find the target dynamics relative to the UAV, we use a spherical coordinate frame. Figure 2 shows the spatial relationship between a target and a UAV in a three dimensional space.

A. UAV Dynamics

We first find a kinematic model of the UAV to develop corresponding guidance laws. Letting $(p_n, p_e, p_d)^T$ be the position of the UAV in the inertial North-East-Down (NED) coordinate frame, V_g be the ground speed, χ be the course angle, γ be the flight path angle, g be the gravitational constant at Earth sea level, and ϕ be the roll angle. The equations for UAV motion then can be written as

$$\begin{aligned} \dot{p}_n &= V_g \cos\chi\cos\gamma, && (3)\\ \dot{p}_e &= V_g \sin\chi\cos\gamma, && (4)\\ \dot{p}_d &= -V_g \sin\gamma, && (5)\\ \dot{\chi} &= \frac{g}{V_g}\tan\phi, && (6)\\ \dot{V}_g &= \alpha_{V_a}\left(V_g^c - V_g\right), && (7)\\ \dot{\gamma} &= \alpha_{\gamma_a}\left(\gamma^c - \gamma\right), && (8)\\ \dot{\phi} &= \alpha_{\phi}\left(\phi^c - \phi\right), && (9) \end{aligned}$$

where α_{V_a}, α_{γ_a}, α_{ϕ} are constant positive control gains. Assuming the wind speed of zero and when the UAV flies toward a target, the ground speed, V_g, is assumed to be constant, i.e., $\dot{V}_g = 0$.

B. Target dynamics relative to the vehicle-1 frame $\mathcal{F}^{v1}$

Let r be the three dimensional distance between the target and the UAV, η and ξ be the azimuth and elevation angles of the target relative to the UAV in the vehicle-1 frame $\mathcal{F}^{v1}$, respectively. The motion equations of the target relative to the UAV in terms of the range, azimuth, and elevation angles are given by [11]

$$\begin{aligned} \dot{r} &= -V_g\left(\cos\gamma\cos\eta\cos\xi + \sin\gamma\sin\xi\right), && (10)\\ \dot{\eta} &= \frac{V_g}{r}\frac{\cos\gamma\sin\eta}{\cos\xi} - \dot{\chi}, && (11)\\ \dot{\xi} &= \frac{V_g}{r}\left(\cos\gamma\cos\eta\sin\xi - \sin\gamma\cos\xi\right). && (12) \end{aligned}$$

Defining $\rho \triangleq V_g/r$, Equations (10)-(12) can be rewritten as

$$\begin{aligned} \dot{\rho} &= \rho^2\left(\cos\gamma\cos\eta\cos\xi + \sin\gamma\sin\xi\right), && (13)\\ \dot{\eta} &= \rho\frac{\cos\gamma\sin\eta}{\cos\xi} - \dot{\chi}, && (14)\\ \dot{\xi} &= \rho\left(\cos\gamma\cos\eta\sin\xi - \sin\gamma\cos\xi\right). && (15) \end{aligned}$$

The control objective is to find input ϕ and γ such that η and $\gamma - \xi$ converge to zero.

Remark: We assume the angle of attack is zero. That is, the direction of the UAV velocity and the x-axis of the body frame aligns in the same direction. Thus the pitch angle and the flight path angle of the UAV are identical, i.e., $\theta = \gamma$.

C. Calculation of η and ξ

Let f be the focal length in units of pixels and λ be the scale converting pixels to meters and assume that each pixel and the pixel array are square. If the width of the square pixel array in units of pixels is M and the field-of-view of

the camera, ν, is known, then the focal length f can be expressed as

$$f = \frac{M}{2\tan\left(\frac{\nu}{2}\right)}.$$

Given the pixel location of the target in an image, (ϵ_x, ϵ_y), the location of the target in the camera frame $\mathbf{p}^c$ is given by $\mathbf{p}^c = (\lambda\epsilon_x, \lambda\epsilon_y, \lambda f)$. The target location in the vehicle-1 frame can be calculated by

$$\mathbf{p}^{v1} = R_{v2}^{v1} R_b^{v2} R_g^b R_c^g \mathbf{p}^c.$$

Then η and ξ can be obtained by

$$\begin{aligned} \eta &= \text{atan2}\left(\mathbf{p}^{v1}(2), \mathbf{p}^{v1}(1)\right), \\ \xi &= -\tan^{-1}\left(\frac{\mathbf{p}^{v1}(3)}{\sqrt{\mathbf{p}^{v1}(1)^2 + \mathbf{p}^{v1}(2)^2}}\right). \end{aligned}$$

IV. Guidance Law Design Using Range Estimation

This section presents the derivation of a guidance law using a Lyapunov-based backstepping technique.

A. Guidance law derivation

The guidance law is based on the following theorem we developed.

Theorem 1: *Consider the nonlinear system described in Equations (13) to (15) with the above associated definitions. If the roll angle, ϕ, and the rate of the flight path angle,$\dot{\gamma}$, are selected as*

$$\phi = \tan^{-1}\left(\frac{V_g}{g}\left(\rho\frac{\cos\gamma\sin\eta}{\cos\xi} + k_1\eta\right)\right), \quad (16)$$

$$\dot{\gamma} = \rho\left(\cos\gamma\cos\eta\sin\xi - \sin\gamma\cos\xi\right) + k_2\left(\xi - \gamma\right), \quad (17)$$

where k_1 and k_2 are positive control gains, then η and $\gamma - \xi$ exponentially converge to zero.

Proof: Defining a Lyapunov function candidate as

$$V \triangleq \frac{1}{2}\eta^2 + \frac{1}{2}\left(\xi - \gamma\right)^2, \quad (18)$$

we can calculate the time derivative of V as

$$\begin{aligned} \dot{V} &= \eta\dot{\eta} + (\xi - \gamma)\left(\dot{\xi} - \dot{\gamma}\right) \\ &= \eta\left(\rho\frac{\cos\gamma\sin\eta}{\cos\xi} - \frac{g}{V_g}\tan\phi\right) \\ &\quad + (\xi - \gamma)\left(\rho\left(\cos\gamma\cos\eta\sin\xi - \sin\gamma\cos\xi\right) - \dot{\gamma}\right). \end{aligned}$$

Selecting ϕ and $\dot{\gamma}$ as in Equations (16) and (17), we have

$$\dot{V} = -k_1\eta^2 + k_2\left(\xi - \gamma\right)^2.$$

■

B. Range estimation

Images captured by a monocular camera do not directly provide the information of the range between an object (shown in an image) and the camera, while bearing information can be easily calculated. To generate the range information required by the controller (16) and (17), we developed an Extended Kalman Filter (EKF) to estimate ρ using the measurements of the azimuth angle, η, and the elevation angle, ξ.

1) Extended Kalman Filter: Selecting the system state as $\mathbf{x} = (\rho, \eta, \xi)^T$, system output as $\mathbf{y} = (\eta, \xi)^T$, and the system input vector as $\mathbf{u} = (\phi, \gamma)^T$, the system dynamics is given by

$$\begin{aligned} \dot{\mathbf{x}} &= f(\mathbf{x}, \mathbf{u}) + \mathbf{q} \quad (19) \\ \mathbf{y} &= h(\mathbf{x}) + \mathbf{w}, \quad (20) \end{aligned}$$

where

$$\begin{aligned} f(\mathbf{x}, \mathbf{u}) &= \begin{pmatrix} \rho^2\left(\cos\gamma\cos\eta\cos\xi + \sin\gamma\sin\xi\right) \\ \frac{\rho\cos\gamma\sin\eta}{\cos\xi} - \dot{\psi} \\ \rho\left(\cos\gamma\cos\eta\sin\xi - \sin\gamma\cos\xi\right) \end{pmatrix}, \\ h(\mathbf{x}) &= \begin{pmatrix} \eta \\ \xi \end{pmatrix}, \end{aligned}$$

Symbol $\mathbf{q}$ is the process noise, representing modeling error and disturbances on the system, and $\mathbf{w}$ is the measurement noise, representing noise on the sensors [10]. The random variables $\mathbf{q}$ and $\mathbf{w}$ are zero-mean Gaussian random processes with covariances Q and R, respectively.

Defining the estimated state of $\mathbf{x}$ as $\hat{\mathbf{x}}$ and the estimation covariance as P, the prediction step of the Kalman filter is given by

$$\begin{aligned} \dot{\hat{\mathbf{x}}} &= f(\hat{\mathbf{x}}, \mathbf{u}), \\ \dot{P} &= AP + PA^T + Q, \end{aligned}$$

where

$$A = \frac{\partial f}{\partial \mathbf{x}} = \begin{pmatrix} A_{11} & A_{12} & A_{13} \\ A_{21} & A_{22} & A_{23} \\ A_{31} & A_{32} & A_{33} \end{pmatrix}$$

and

$$\begin{aligned} A_{11} &= 2\rho\left(\cos\gamma\cos\eta\cos\xi + \sin\gamma\sin\xi\right), \\ A_{12} &= -\rho^2\left(\cos\gamma\sin\eta\cos\xi\right), \\ A_{13} &= \rho^2\left(-\cos\gamma\cos\eta\sin\xi + \sin\gamma\cos\xi\right), \\ A_{21} &= \frac{\cos\gamma\sin\eta}{\cos\xi}, \\ A_{22} &= \frac{\rho\cos\gamma\cos\eta}{\cos\xi}, \\ A_{23} &= \frac{\rho\cos\gamma\sin\eta\sin\xi}{\cos^2\xi}, \\ A_{31} &= \cos\gamma\cos\eta\sin\xi - \sin\gamma\cos\xi, \\ A_{32} &= -\rho\cos\gamma\sin\eta\sin\xi, \\ A_{33} &= \rho\left(\cos\gamma\cos\eta\cos\xi + \sin\gamma\sin\xi\right). \end{aligned}$$

Defining the Kalman gain at time step k as L_k, when a measurement is available, the update step of the Kalman filter is given by

$$\begin{aligned} L_k &= P_k^- C^T\left(CP_k^- C^T + R\right)^{-1} \\ P_k^+ &= \left(I - L_k C\right)P_k^- \\ \hat{\mathbf{x}}^+ &= \hat{\mathbf{x}}^- + L_k\left(\mathbf{y}_k - h\left(\hat{\mathbf{x}}^-\right)\right), \end{aligned}$$

where the superscripts $-$ and $+$ represent the variable values obtained before and after the update step, respectively.

Subscript k represents the time step when the variable values are obtained, I is an identity matrix and

$$C = \frac{\partial h}{\partial \mathbf{x}} = \begin{pmatrix} 0 & 1 & 0 \\ 0 & 0 & 1 \end{pmatrix}.$$

2) Observability Analysis: To investigate the performance of the EKF developed in the previous section on estimating ρ using the measurements of η and ξ, the following lemma comes in handy.

Lemma 1 [11]: *The target state (ρ, η, ξ), whose motion is governed by Equations (19) and (20), is observable at time t if and only if at least one of the following three conditions is satisfied: (1) $\eta(t) \neq 0$; (2) $\xi(t) \neq \theta(t)$; or (3) $\phi(t) \neq 0$.*

In vision-based target tracking problems, we typically aim to push the target shown in the image toward the center of the camera view in order to maximize the probability of observing the target in the future, giving maximum time for the target to move out of the sensor FOV. This objective, however, would result in $\eta = 0$, $\xi = \theta$, $\phi = 0$, implying that the state is not observable. In the forthcoming simulation results, we show the estimation results when the control law moved the vehicle to push the target toward the center of the image plane. Developing observers, estimators, and control laws that collectively prevent the unobservability condition will be conducted during second quarter of the project period. In addition, we will be performing a comparative study to evaluate the performance of the control method in this section with the one shown below, a method that does not depend on any range estimations, during the same period.

V. Guidance Law Design Without Using Range Information

The guidance law developed in Section IV requires the estimation of range, which induces estimation error and computation inaccuracy. This section introduces another guidance law we developed that does not use range information. The control law is based on a sliding mode technique that constrains the motion of a system to the manifold $s_1 = \eta = 0$ and $s_2 = \xi - \gamma = 0$, i.e., $\gamma = \xi$. The UAV motion on the manifold is independent of ρ. The objective, then, is to transform the system states to desired points on the manifold.

Theorem 2: *Consider the nonlinear system described in Equations (13) to (15) with the associated definitions defined earlier. If the roll angle, ϕ, and the rate of the flight path angle,$\dot{\gamma}$, are selected as*

$$\phi = \tan^{-1}\left(\frac{V_g}{g}\left(\rho_{max}\left|\frac{\cos\gamma\sin\eta}{\cos\xi}\right| + B_\phi\right)\text{sat}\left(\frac{\eta}{\delta_\eta}\right)\right), \tag{21}$$

$$\begin{aligned}\dot{\gamma} &= (\rho_{max}\left|\cos\gamma\cos\eta\sin\xi\right. \\ &\quad \left. - \sin\gamma\cos\xi\right| + B_\gamma)\,\text{sat}\left(\frac{\xi-\gamma}{\delta_\gamma}\right),\end{aligned} \tag{22}$$

$$\text{sat}(\mu) \triangleq \begin{cases} \text{sgn}(\mu), & |\mu| > 1, \\ \mu, & otherwise, \end{cases}$$

then η and $\gamma - \xi$ exponentially converge to zero, where ρ_{max} is a positive constant, representing the maximum value of ρ. B_ϕ and B_γ are constants preventing ϕ and $\dot{\gamma}$ from being stuck at zero when η and $\gamma - \xi$ are zeros, δ_η and δ_γ are slope constants of a saturation function, sat$(\cdot)$ denotes a saturation function and sgn$(\cdot)$ stands for the sign of the argument.

Proof: Defining a Lyapunov function candidate $W \triangleq \frac{1}{2}s_1^2 + \frac{1}{2}s_2^2$, where $s_1 = \eta$ and $s_2 = \xi - \gamma$, we can calculate the time derivative of W as

$$\begin{aligned}\dot{W} &= s_1\dot{\eta} + s_2\left(\dot{\gamma} - \dot{\xi}\right) \\ &= s_1\left(\rho\frac{\cos\gamma\sin\eta}{\cos\xi} - \frac{g}{V_g}\tan\phi\right) \\ &\quad + s_2\left(\rho\left(\cos\gamma\cos\eta\sin\xi - \sin\gamma\cos\xi\right) - \dot{\gamma}\right) \\ &\leq |s_1|\,\rho_{max}\left|\frac{\cos\gamma\sin\eta}{\cos\xi}\right| - s_1\frac{g}{V_g}\tan\phi \\ &\quad + |s_2|\,\rho_{max}\left|\cos\gamma\cos\eta\sin\xi - \sin\gamma\cos\xi\right| - s_2\gamma,\end{aligned}$$

where $\rho_{max} > 0$ is the upper bound of ρ. Selecting ϕ and $\dot{\gamma}$ as in Equations (21) and (22), we have

$$\begin{aligned}\dot{W} &\leq -B_\phi|\eta| - B_\theta|\xi - \gamma| < 0, \\ &\quad \forall\,|\eta| > \delta_\eta \text{ and } \forall\,|\xi - \gamma| > \delta_\gamma.\end{aligned}$$

Therefore, when $|\eta| > \delta_\eta$ and $|\xi - \gamma| > \delta_\gamma$, $|s_1|$ and $|s_2|$ are strictly decreasing until they reach the set $\{|s_1| \leq \delta_\eta\}$ and $\{|s_2| \leq \delta_\gamma\}$ in finite time and remain inside thereafter, resulting $|\eta| \leq \delta_\eta$ and $|\xi - \gamma| \leq \delta_\gamma$.

■

VI. Simulation Results

In this section, we show the results of simulations conducted in the MATLAB/Simulink environment to verify the effectiveness of the developed guidance laws presented in Sections IV and V. We refer GL_{range} and $GL_{sliding}$ as the results generated when either the guidance laws based on range estimation or the sliding mode technique was used, respectively. The target starts from location $(100, 0)$ m in the North-East coordinate frame. The UAV starts at $(0, 500, 100)$ m. The constant target speed is 10 m/s and the constant UAV speed is 15 m/s.

A. Results using the guidance law based on range estimation

This section shows the results generated using the guidance law based on range estimation. Figure 4 shows the top-down view of the trajectories of the UAV (solid blue) and the target (dashed red). Figure 5 illustrates the evolution of the UAV inputs, and Figure 6 shows the target trajectory in the camera view and the corresponding evolution of the target motion and its distance to the center of the image. It can be seen that the target trajectory in the camera view is close to the center of the image except the relatively large oscillation before 10 seconds. Figure 7 shows the estimated (dashed red) and actual (solid blue) distance between the target and the UAV. The estimated range does not converge to its real value due to the unobservability of the system state when the UAV was flying toward the target. Although the controller uses an inaccurate range information, the large value of the range results in a very small value of ρ,

which attenuates the contribution of the terms, $\frac{\cos\gamma\sin\eta}{\cos\xi}$ and $\cos\gamma\cos\eta\sin\xi - \sin\gamma\cos\xi$, turning the guidance law into a controller similar to the PID controller.

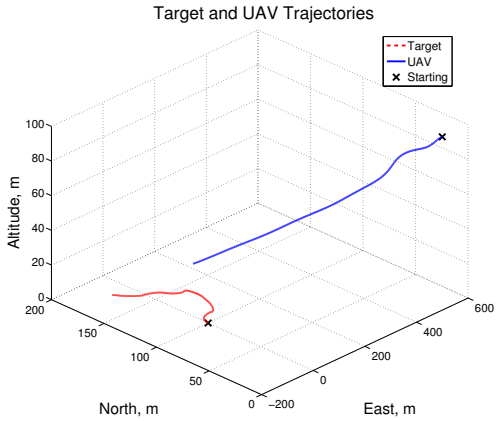

Fig. 4: Top-down view of the trajectories of the UAV and the target using GL_{range}.

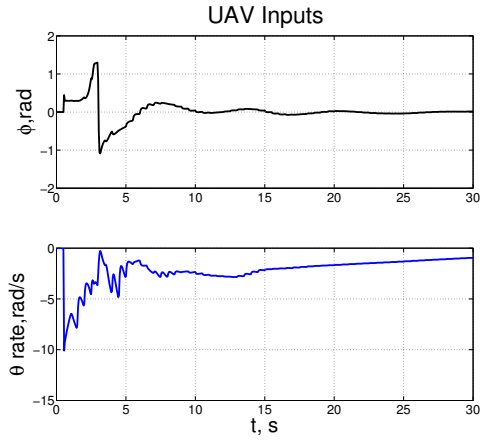

Fig. 5: UAV control inputs using GL_{range}.

B. Results using the guidance law without using range information

This section shows the results generated using the guidance law based on the sliding mode technique. Figure 8 shows the top-down view of the trajectories of the UAV (solid blue) and the target (dashed red). Figure 9 illustrates the evolution of the inputs of the UAV. Figure 10 shows the target trajectory in the camera view and the corresponding target motions and its range to the center of the image plane. It can be seen that the target trajectory in the camera view is close to the center of the image plane and has less oscillations than the ones shown in Figure 6.

VII. Conclusion

In this paper, we developed two novel guidance laws which incorporate relative motions of a UAV and a ground target by either estimating the distance between a UAV and a ground target using camera measurements or by using the sliding mode control technique and camera measurements. The observability analysis was conducted to evaluate the performance of the technique to estimate the UAV-to-target range. The simulation results show the effectiveness of the two guidance laws as both try to push the target toward the center of the image plane by maneuvering the UAV motion.

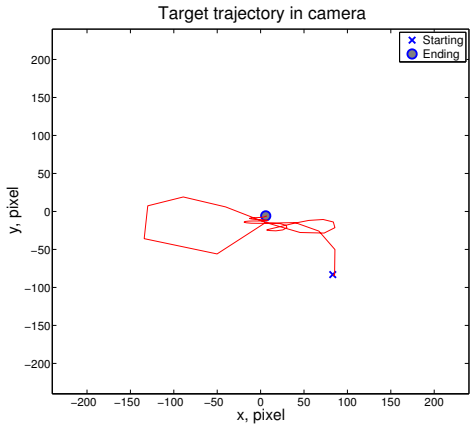

(a) Target trajectory in camera.

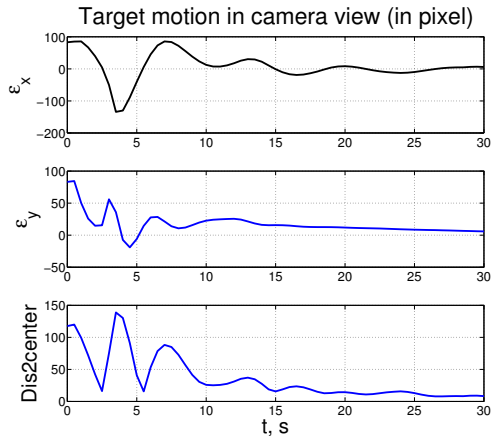

(b) Target coordinate evolution.

Fig. 6: Target motion in the camera view and corresponding evolutions of the coordinates using GL_{range}.

References

[1] L. Sun and D. Pack, "Mobile target tracking using an unmanned aerial vehicle with a non-gimbaled video sensor," in *AIAA SciTech*. American Institute of Aeronautics and Astronautics, Jan. 2015, pp. –. [Online]. Available: http://dx.doi.org/10.2514/6.2015-1077

[2] J. Kim and Y. Kim, "Moving ground target tracking in dense obstacle areas using UAVs," in *Proceedings of the 17th World Congress: The International Federation of Automatic Control*, Seoul, Korea, July 6-11 2008, pp. 8552–8557.

[3] R. Rysdyk, "Unmanned aerial vehicle path following for target observation in wind," *AIAA Journal of Guidance, Control, and Dynamics*, vol. 29, no. 5, pp. 1092–1110, 2006.

[4] V. N. Dobrokhodov, I. I. Kaminer, K. D. Jones, and R. Ghabcheloo, "Vision-based tracking and motion estimation for moving targets using small UAVs," in *Proceedings of the 2006 American Control Conference*, Minneapolis, Minnesota, USA, June 14-16 2006, pp. 1428–1433.

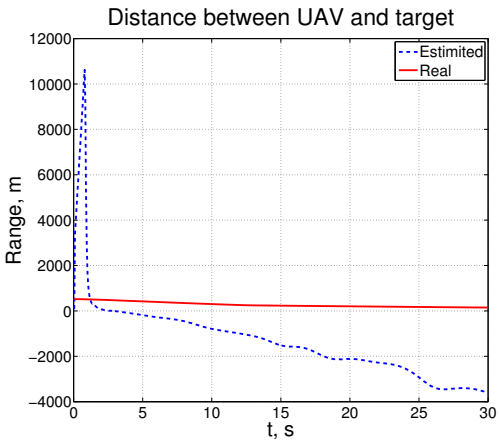

Fig. 7: Estimated and real distances between the UAV and the target using GL_{range}.

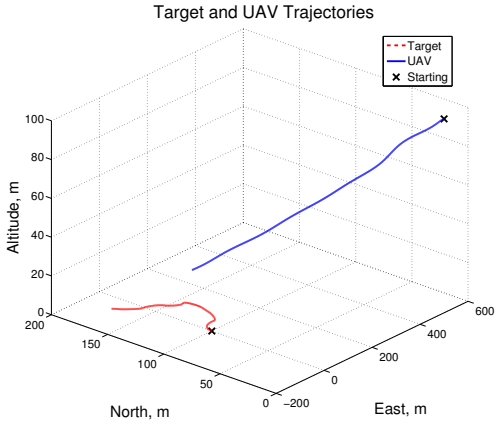

Fig. 8: Top-down view of the trajectories of the UAV and the target using $GL_{sliding}$.

[5] P. Theodorakopoulos and S. Lacroix, "A strategy for tracking a ground target with a uav." in *IROS*, 2008, pp. 1254–1259.

[6] F. Rafi, S. Khan, K. Shafiq, and M. Shah, "Autonomous target following by unmanned aerial vehicles," in *Proc. SPIE 6230, Unmanned Systems Technology VIII, 623010*, May 2006.

[7] E. W. Frew, X. Xiao, S. Spry, T. McGee, Z. Kim, J. Tisdale, R. Sengupta, and J. K. Hedrick, "Flight demonstrations of self-directed collaborative navigation of small unmanned aircraft," in *AIAA 3rd "Unmanned Unlimited" Technical Conference, Workshop and Exhibit*, no. AIAA 2004-6608, Chicago, Illinois, USA, 20 - 23 September 2004.

[8] B. R. Geiger, J. F. Horn, G. L. Sinsley, J. A. Ross, L. N. Long, and A. F. Niessner, "Flight testing a real-time direct collocation path planner," *Journal of Guidance, Control, and Dynamics*, vol. 31, no. 6, pp. 1575–1586, 2008.

[9] J. Saunders and R. Beard, "Visual tracking in wind with field of view constraints," *International Journal of Micro Air Vehicles*, vol. 3, no. 3, pp. 169–182, 2011.

[10] R. W. Beard and T. W. McLain, *Small Unmanned Aircraft: Theory and Practice*. Princeton University Press, 2012.

[11] H. Yu and R. Beard, "Vision-based local-level frame mapping and planning in spherical coordinates for miniature air vehicles," *Control Systems Technology, IEEE Transactions on*, vol. 21, no. 3, pp. 695–703, May 2013.

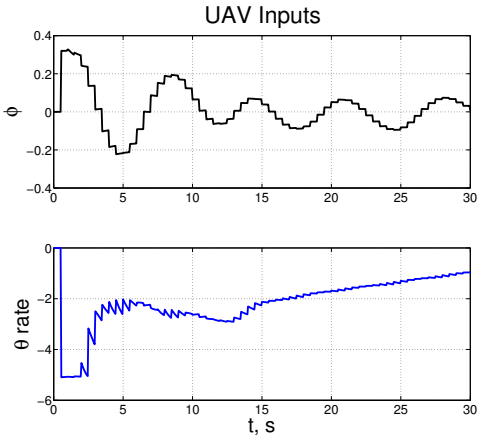

Fig. 9: UAV control inputs using $GL_{sliding}$.

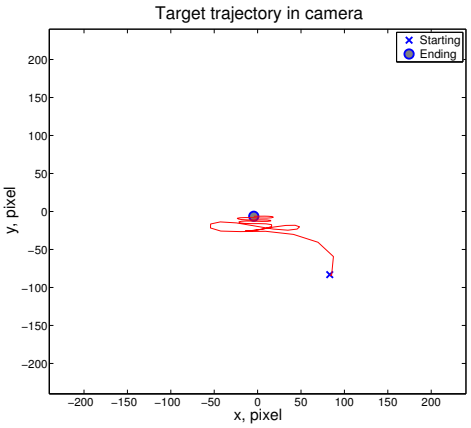

(a) Target trajectory in camera.

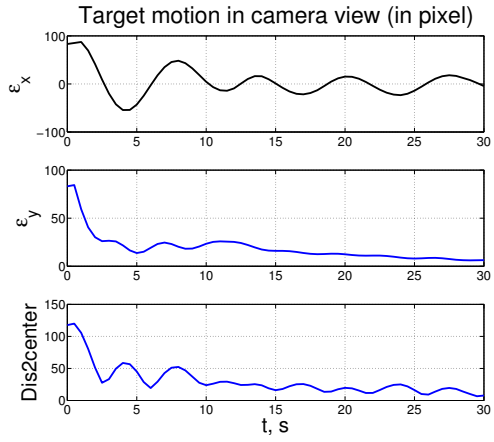

(b) Target coordinate evolution.

Fig. 10: Target motion in the camera view and corresponding evolutions of the coordinates using $GL_{sliding}$.